

---

This is an electronic reprint of the original article.  
This reprint may differ from the original in pagination and typographic detail.

Billah, Md Masum; Martin, Floran; Belahcen, Anouar

## A computationally effective method for iron loss estimation in a synchronous machine from a static field solution

*Published in:*

Proceedings of the 2020 International Conference on Electrical Machines, ICEM 2020

*DOI:*

[10.1109/ICEM49940.2020.9271020](https://doi.org/10.1109/ICEM49940.2020.9271020)

Published: 23/08/2020

*Document Version*

Peer-reviewed accepted author manuscript, also known as Final accepted manuscript or Post-print

*Please cite the original version:*

Billah, M. M., Martin, F., & Belahcen, A. (2020). A computationally effective method for iron loss estimation in a synchronous machine from a static field solution. In *Proceedings of the 2020 International Conference on Electrical Machines, ICEM 2020* (pp. 751-757). Article 9271020 (Proceedings (International Conference on Electrical Machines)). IEEE. <https://doi.org/10.1109/ICEM49940.2020.9271020>

---

This material is protected by copyright and other intellectual property rights, and duplication or sale of all or part of any of the repository collections is not permitted, except that material may be duplicated by you for your research use or educational purposes in electronic or print form. You must obtain permission for any other use. Electronic or print copies may not be offered, whether for sale or otherwise to anyone who is not an authorised user.

© 2020 IEEE. This is the author's version of an article that has been published by IEEE. Personal use of this material is permitted. Permission from IEEE must be obtained for all other uses, in any current or future media, including reprinting/republishing this material for advertising or promotional purposes, creating new collective works, for resale or redistribution to servers or lists, or reuse of any copyrighted component of this work in other works.

# A Computationally Effective Method for Iron Loss Estimation in a Synchronous Machine from a Static Field Solution

Md Masum Billah, Floran Martin, and Anouar Belahcen, *Senior Member, IEEE*

**Abstract**—In this paper, a computationally effective iron loss calculation method for synchronous machines is presented. The method is based on a single static 2D finite element field solution in the machine cross-section, which makes it much faster than the one based on the time-stepping solution. The developed method is applied to a salient pole synchronous machine, and the computational accuracy is validated against the time-stepping method. The proposed iron losses computation method showed a fair accuracy and a considerable speed-up of the computations. It can be an excellent alternative for the iron losses estimation in the optimization procedure of synchronous machines, where a considerable amount of finite element solutions needs to be carried out. Besides the losses comparison, local reconstruction of the time dependency of other quantities such as the magnetic vector potential and the magnetic flux density is reported for a better understanding of the method.

**Index Terms**—dynamic field solution, finite element method, iron losses, synchronous machine, static field solution, time-stepping method.

## I. INTRODUCTION

OWING to the increasing energy demand, highly efficient synchronous machines play a crucial role in energy saving by reducing energy consumption. Like other electrical machines, power losses are a common issue in a synchronous machine, which increases the temperature and degrades the performance by affecting the maximum output power. Besides, extreme temperature rise can lead to insulation failure, consequently, decrease the life expectancy of a synchronous machine. Power losses can be segregated into Joule losses in the winding of the machine, the iron losses in the core of the machines, the frictions, and mechanical losses, and the permanent magnet losses, which are due to eddy currents in these parts if any. Usually, the Joule and friction losses can be estimated from static quantities, such as the rotational speed and the supply currents, but the iron and permanent magnet losses require the temporal and spatial distribution of the magnetic flux density in the corresponding parts of the machine.

This work was supported by the internal funding from computational electromechanics group at Aalto University, Finland.

M. M. Billah, F. Martin, and A. Belahcen are with Aalto University, Department of Electrical Engineering and Automation, Espoo, Aalto-00076 Finland (e-mail: md.billah@aalto.fi, floran.martin@aalto.fi, anouar.belahcen@aalto.fi)

A. Belahcen is also with Tallinn University of Technology, Tallinn, Estonia.

The magnetic flux density in the electrical machine is three-dimensional, and solving a three-dimensional problem is still laborious. The solution becomes much easier if the problem domain is simplified to the two-dimensional model where the machine geometry and material equations are independent of the coordinate parallel to the machine shaft, i.e., z-coordinate. A detailed description of the 2D finite element method and its application on solving two-dimensional electromagnetic fields problem is demonstrated in [1] among others. Moreover, the effects of armature reaction and the magnetizing field, the slotted nature of the machine, and the highly distorted magnetic field appearing from the permanent magnet cause the non-sinusoidal and time-varying distribution of the magnetic flux density at different locations of the machine's core. As a result, the solution of the magnetic flux density distribution is usually achieved for each time step through the time-stepping method [2]. In addition, the magnetic flux density in the rotating machine is not a single frequency component anymore and contains higher frequency components.

A common practice of the iron losses computation is to obtain the flux density distribution from the time-stepping finite element simulation and calculate the losses in the post-processing stage through the Fourier decomposition of the flux density waveform over one period [3], [4]. The solution accuracy of the time-stepping method depends on the size of the time step, and a smaller step size usually ensures better accuracy. Moreover, the steady-state characteristics are often desirable for the iron losses computation, which requires to run the machine at least for a few electrical periods. A suitable time resolution selection for the dynamic analysis and the effect of it on the solution accuracy is a separate topic, and no exact recommendation was found. For instance, the number of time steps per period and the number of electrical periods were used by [5], [6] 300-1000 steps per period and 2-10 electrical periods, respectively. However, all these factors lead to high computational cost for achieving the dynamic solution; consequently, the iron losses computation from this solution. The difference is more visible when the iron losses computation from the dynamic solution required 35.07 s, and from a single static simulation needed only 0.512 s. Despite the high computational cost, the time-stepping method is more conventional and still a popular choice for the iron losses computation. This is probably because the conventional loss computation method

provides better accuracy and also stays productive as long as the number of computations remains in a reasonable range. However, the situation is different when an excessive number of computations are required, e.g., machine optimization, which turns this method into unprofitable by increasing the simulation time. In such a case, the computation of the iron losses from a time-efficient static solution is more than justified.

Early on, a series of thirty static field solutions were computed in [7] by moving the rotor at one slot pitch interval over one electrical period, and the resulting field solutions were used to estimate the stator core losses. A similar approach has been used in [8] with a smaller number of snapshots, i.e., static field solutions than [7]. The method presented in [7], [8] was extended by [9] in order to take the rotor core losses into account. A simplified, i.e., surrogate finite element method is introduced in [10] to reduce the requirements of the number of successive snapshots, i.e., static field solutions. However, the method presented in [10] is particularly developed for the interior permanent magnet machine with concentrated, i.e., non-overlapping coils. Another snapshot-based computationally effective finite element model is developed in [11] and applied for the optimization process of the interior permanent magnet machine. The proposed methods in [10], [11] significantly reduced the requirements of the number of static simulations, i.e., 2-5 solutions required, respectively for the iron losses computation compared to the methods presented in [7], [8], [9]. A major drawback of these snapshot-based methods is that accuracy and precision are highly influenced by the number of static simulations taken into consideration. Adding more static field solutions may make sure better accuracy; however, it also increases the computational cost. Also, no specific benchmark is noticed for the exact requirements of the number of static simulations.

An ultrafast static field computation method has been presented in [5], by coupling the static field equations and space vector model within the same finite element solution. The method has given accurate results from a single static simulation compared to the measurement and time-stepping method. Modeling a fast and accurate static field computation method is an independent topic of research by itself, which is out of the scope of this paper. Instead, our main goal is to develop the iron losses computation method by using the readily available static field computation method presented in [5], which can be an alternative method of the iron losses computation from the dynamic field solution in many applications. In this paper, the accuracy and computational cost of the developed method are validated with the conventional time-stepping method extensively.

The presented iron losses computation method in this paper outperforms the previously developed computationally effective static iron losses calculation methods in [7], [8], [9], [10], [11] several ways. Here, the iron losses are computed from a single static simulation, and no rotor motion is taken into account. Hence, the accuracy of this method is not restricted to the requirements of the number of static sim-

ulations. Furthermore, this paper solely and comprehensively deals with developing an ultrafast iron loss computation technique, which can overcome the above-mentioned snapshot-based methods in terms of computational cost and also can compete with them in terms of accuracy. Moreover, the proposed iron losses computation method is not limited to a particular synchronous machine and applicable to any kind of synchronous machine.

## II. METHODOLOGY

### A. Iron Loss Model

In this proposed method, the iron losses will be computed from the Fourier decomposition of the flux density waveform over one period. A suitable and accurate iron loss model requires to compute the losses from the peak values of the flux density at each harmonic component. Moreover, the selected iron loss model can be easily integrated with the static or dynamic finite element solution in the post-processing stage. The empirical iron loss models are fast, easy to implement, and applicable for the iron losses estimation roughly [12]. However, many researchers have extended the empirical iron loss models and estimated the iron losses conventionally with relatively good accuracy [13], [14]. The modified Jordan loss separation model presented in [15] is adopted for the iron losses computation

$$P_{hys} = \int_{V_c} \left( \sum_{n=1}^N C_{hys}(n\omega_s) \hat{B}_n^2 \right) dV \quad (1)$$

$$P_{ed} = \int_{V_c} \left( \sum_{n=1}^N C_{ed}(n\omega_s)^2 \hat{B}_n^2 \right) dV \quad (2)$$

where  $P_{hys}$  and  $P_{ed}$  represents the hysteresis loss and eddy current loss, respectively.  $C_{hys}$  and  $C_{ed}$  expresses the hysteresis and eddy current loss coefficients,  $\omega_s$  stands for the angular frequency of the supply,  $V_c$  is the volume of the stator iron core, and  $\hat{B}_n$  is the peak flux density value at  $n^{th}$  harmonic components. However, the modified iron loss model in Equations 1, and 2 also suffers from some shortcomings. For instance, two-loss coefficients  $C_{hys}$  and  $C_{ed}$  were computed from the Epstein frame test, and no differentiation was made between the alternating and rotational fields [16]. Moreover, the minor hysteresis loops were not taken into consideration properly. In the statistical loss segregation method, the classical eddy current loss and excess loss are presented separately. However, the computation of the excess loss coefficient through the Epstein frame test is difficult as it does not allow us to identify the difference between the eddy current due to the classical loss and excess loss [17]. Alternatively, a two-term iron loss separation method is developed as shown in Equations 1, and 2 where the classical eddy current loss and excess loss are combined and formed a global eddy current loss,  $P_{ed}$  in Equation 2. It can be noted that the same iron loss model is also used to compute the losses through the time-stepping method. An in-house 2D finite element solver software FCSMEK has been

developed by the electromechanics research group at Aalto University and is used to compute the iron losses from the proposed method and the conventional time-stepping method.

### B. Time Dependence of the Flux Density from the Static Analysis

In finite element method, the flux density  $\mathbf{B}$  values are computed natively in the  $x$ - $y$  coordinates; thus, the actual iron losses are calculated from the flux density components  $B_x$  and  $B_y$  values. In practice, the flux density  $\mathbf{B}$  is solved by assuming the two-dimensional approximation where the flux density lies only in  $(x, y)$  plane in Cartesian coordinates or  $(r, \phi)$  plane in cylindrical coordinates and does not depend on the  $z$ -axis. The flux density components  $B_x$  and  $B_y$  can be calculated from the partial derivation of magnetic vector potential values with respect to the  $x$ - $y$  coordinates. The existence of space harmonic components in case of sinusoidal voltage supply in the electrical machine affects the flux density waveform and influence to depend on time. However, the obtained flux density  $\mathbf{B}$  values from a static field solution is independent of time, i.e., static. The time dependence of the static flux density waveform needs to be introduced in order to compute the iron losses. In FCSMEK, the stator finite element mesh is constructed by multiplying the slot pitch mesh. Thus, the number of elements in one slot pitch mesh is repeated to the next slot pitches, and elements from one slot pitch to another has the same position and size. Therefore, the space variation of the static flux density waveform both for the stator yoke and teeth over one period can be achieved by selecting the elements at one slot pitch interval. The stator slot pitch is computed as follows

$$\theta_s = \frac{2\pi}{Q_s} \quad (3)$$

where  $\theta_s$  is the stator slot pitch, and  $Q_s$  denotes the total number of stator slots. The time dependence of the flux density waveform can be achieved by assuming that the flux density waveform is moving with the fundamental angular frequency  $\omega$  and time  $t$ . The time step for the time dependence is computed as follows

$$\Delta t = \frac{\Delta\theta_s p}{\omega} \quad (4)$$

where  $p$  denotes the number of pole pairs,  $\theta_s$  is the stator slot pitch, and  $\omega$  is the supply angular frequency. At any instant of angular distance  $\theta$  and time  $t$ , the displacement of the moving flux density with initial position  $\theta_o$  can be determined as  $\theta = \theta_o + \omega t$ . With respect to the initial position  $\theta_o$  and time  $t_o$ , the displacement of the flux density waveform can be written as

$$\mathbf{B}(\theta, r, t) = \mathbf{R}\mathbf{B}(\theta - \omega t, r, 0) \quad (5)$$

where  $\theta$  is the angular position of the point at which the flux density is estimated and  $r$  its radial position from the rotor midpoint.  $\mathbf{R}$  is the rotation matrix given in Equation 6.

$$\mathbf{R} = \begin{bmatrix} \cos \theta & -\sin \theta \\ \sin \theta & \cos \theta \end{bmatrix} \quad (6)$$

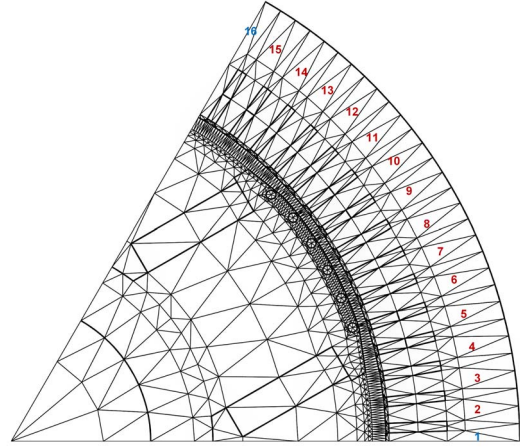


Fig. 1. Element selections for the flux density waveform formation over the solution region in the static analysis.

It should be noted that the radial dependency does not need to be solved in Equation 5. It is intrinsic within the time dependency reconstruction.

### C. Flux Density Waveform Formation in Static Analysis

The process of element selections in the stator yoke at each slot pitch interval is depicted in Figure 1. In such a case, the number of stator slots and the number of points in the flux density waveform should be equal. Similarly, the flux density waveform in the stator teeth is formed by choosing the elements at one slot pitch interval. In such a way, elements to elements flux density waveform are constructed at each slot pitch interval over two pole pitches to calculate the average iron losses from a closed cycle of the flux density waveform using the Equations 1, and 2. The same size element in each stator slot pitch meshes from 2 to 15, i.e., represents full slot pitch is found at a distance of one slot pitch interval. On the other hand, the element in positions 1, and 16 represent half of the slot pitch. The flux density waveform as depicted in Figure 2 was formed by specifying an observation point at one element, i.e., position 1, and varying by one slot pitch from 1 to 16 as shown in Figure 1. As one observation point was specified in each element; hence, no elements were missed. As a result, the flux density points are evenly spaced in Figure 2 even though the element in positions 1, and 16 are different compared to other selected elements. Such variation over the solution region in Figure 1 provides the half cycle of the flux density waveform. A complete cycle of flux density waveform was formed in Figure 2 by mirroring the obtained half cycle of the flux density waveform due to the symmetry of the solution region. A problem was identified during the computation as the element in positions 1, and 16 have different sizes compared to other slot pitch meshes, i.e., 2 to 15. For this reason, the total number of elements in this slot pitch is not equal compared to the other slot pitch meshes. However, the same number of elements in each slot pitch mesh is required when the elements to elements flux

TABLE I  
COMPUTED PARAMETERS COMPARISON BETWEEN THE DYNAMIC AND  
STATIC ANALYSIS.

Parameter	Comp.dynamic	Comp.static
Voltage	3150 V	3150 V
Current	2285 A	2274 A
Frequency	50 Hz	50 Hz
Active power	12.46 MW	12.407 MW
Shaft power	12.42 MW	12.69 MW
Air-gap torque	118.6 kNm	121.2 kNm
Power factor	0.97	0.99
Total elements	2026	2026
Total nodes	4113	4113
Comp. time	35.07 s	0.512 s

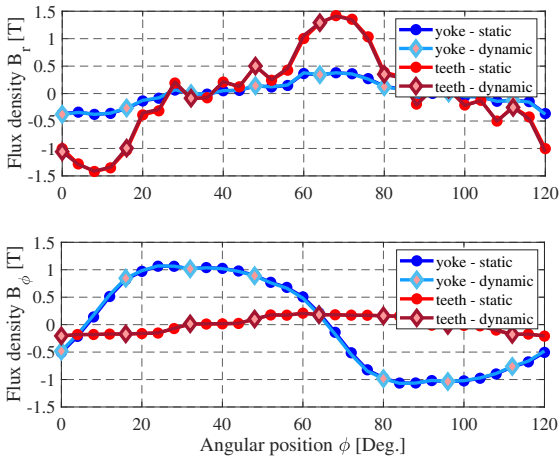


Fig. 2. Space variation of the magnetic flux density over one period in the case of static and dynamic analysis, at the same radial distance from the rotor midpoint.

density waveform need to be formed in the actual iron losses computation. Any asymmetrical slot pitch mesh can result in erroneous results. Therefore, the actual iron losses calculation was continued without taking this slot pitch mesh. Moreover, the recommended integration points in the case of quadratic triangular elements and the corresponding flux density values were considered in the actual iron losses computation.

### III. MODEL APPLICATION IN SYNCHRONOUS MACHINE

#### A. Studied Synchronous Machine and Simulation Parameters

The proposed method has been applied to a 12.5 MW salient pole synchronous machine, which consists of 90 stator slots and six rotor poles. The second-order triangular element having six nodes has been chosen by trading off between the computation time and accuracy. The finite element mesh of the smallest symmetry section is shown in Figure 1, which is used in the simulation. The information about the total elements and nodes of the solution sector is listed in Table I. The machine was supplied from a voltage source and simulated at a specific operating point. The rotor angle and the field winding voltage required for this operating

point was computed through an algorithm developed by the electromechanics research group at Aalto University.

The static finite element solution is achieved through solving the circuit equations of the stator winding based on the two-axis model, and the field equations assuming the steady-state condition. Therefore, the flux density induced in rotor parts is mainly DC in nature, and the complete iron loss is contributed by the stator core in the case of a synchronous machine. Thus, the iron losses only in the stator core are computed by the proposed method and the conventional method for a fair comparison. The non-linearity of the system is solved using the Newton-Raphson iteration method. It is noticeable that such a coupling approach is only possible if the flux linkage distribution is assumed to be sinusoidal variation with time. The machine parameters obtained from a single static simulation are illustrated in Table I.

The dynamic analysis was continued with the same parameters used in the static analysis. The simulation was carried out for 300 steps per period, and four periods were studied to obtain the steady-state operating characteristics. A small step size was chosen for better accuracy, which may increase the computation time slightly. Thus, the user needs to be compromised between the accuracy and the computation cost. The time was discretized into a short time interval using the Crank-Nicholson time-stepping method. The field and the circuit equations were solved for each successive time interval. The non-linearity of the system equations was solved by the Newton-Raphson iteration method. The operating parameters acquired from the dynamic analysis are tabulated in Table I.

It can be seen in Table I that the operating parameters obtained from the static analysis and the dynamic analysis are in relatively good agreement. Some of the parameters such as the terminal current, air-gap torque, shaft power, and power factor were computed from the static analysis slightly different than the dynamic analysis. This is because the steady-state parameters were obtained in the dynamic analysis. On the other hand, the parameters were calculated in the static analysis at the initial state of analysis based on the two-axis model by assuming the steady-state condition. Therefore, the static computation may overestimate or underestimate these parameters slightly.

#### B. Magnetic Flux Density and Harmonics Analysis

Figure 3 shows the flux contour lines and the flux density distribution of the smallest symmetry section in the static analysis. The space distribution of the radial  $B_r$  and tangential  $B_\phi$  components of the flux density values in the stator yoke and teeth at given radial positions from the rotor midpoint over one period for both methods are presented in Figure 2. The formation of flux density waveform in the static analysis is already described in Section II-C. The space distribution of the flux density waveform in the dynamic analysis was formed by defining the observation points at one slot pitch interval, and simulation was carried out for

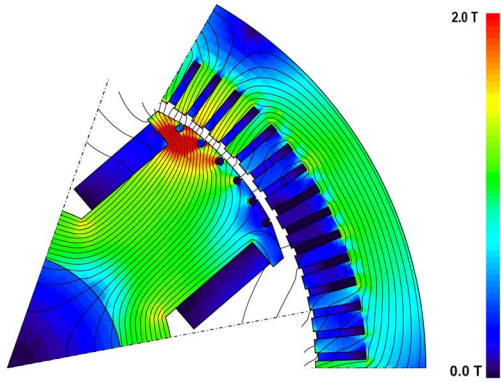


Fig. 3. Flux density distribution of the solution region in the static analysis.

each observation point with 300-time steps per period. The flux density values were chosen at one specific time from the number of simulations of each observation point at the best fitting position. The space variation of the flux density waveform at different moments in dynamic analysis has the same magnitude with a phase shift respecting to the flux density waveform in the static analysis. However, the phase shift has no effect on the iron losses computation as the selected iron loss model in Equations 1, and 2 does not take the phase shift into account. The radial components of the flux density  $B_r$  are higher in the stator teeth, and the tangential components  $B_\phi$  are more elevated in the stator yoke. The non-sinusoidal flux density distribution is noticeable due to the spatial harmonic components present in the waveform.

The Fourier transformation was performed to analyze the harmonic components present in the flux density waveform in Figure 2. The magnitude of flux density  $B$  at each harmonic component was computed, and presented in Figure 4 from the Fourier components of the radial  $B_r$  and tangential  $B_\phi$  flux density waveform. A significant amount of higher harmonic components are appeared in the stator teeth compared to the stator yoke in both methods. The proposed method suffers from some shortcomings as the consideration of the number of harmonic components are limited to the number of stator slots. According to the Nyquist theorem, up to  $7^{th}$  harmonic components can be taken into account for the iron losses calculation from the sampled waveform in the static analysis. However, one possibility to overcome such shortcoming by forming a more dense mesh, hence, more sampling points can be attained in the flux density waveform. Moreover, the impact of rotor motion on the harmonic components were not taken into consideration.

It is mentioned already in Section II-C that the obtained samples are non-uniformly spaced in both spatial and temporal variation due to miss one slot pitch mesh between element in positions 1, and 16. The Nyquist-Shannon sampling theorem works perfectly for the samples that are evenly spaced in time. However, unevenly spaced samples can also be reconstructed as accurately as possible if the average sampling rate follows the Nyquist rule, but the signal may

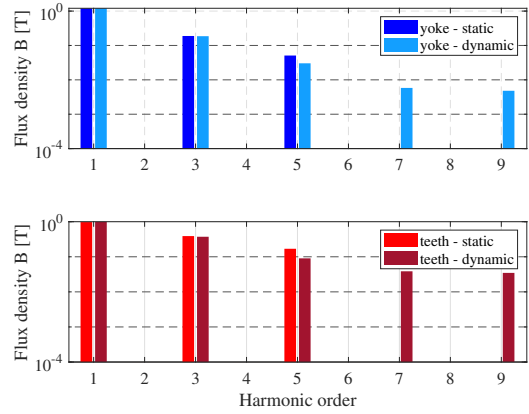


Fig. 4. Magnitude of the flux density at each harmonic component in the static and dynamic analysis: (above) yoke; (below) teeth. Note the logarithm scale for the y-axis.

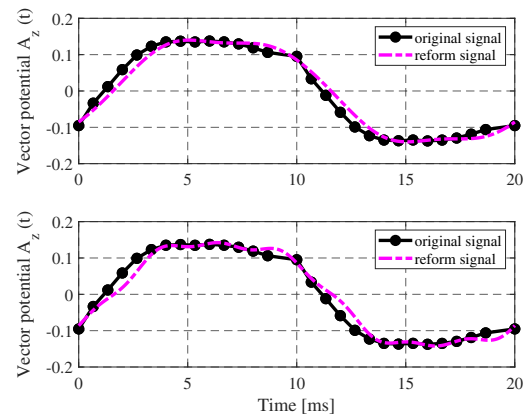


Fig. 5. Magnetic vector potential  $A_z$  signal reconstruction from the Fourier series at different harmonic orders in the case of static analysis: (above) up to the  $5^{th}$  harmonic ; (below) up to the  $7^{th}$  harmonic.

loss one or two samples. Thus, the investigation of including the maximum number of harmonic components in the static loss computation method was carried out by reconstructing the sampled waveform of a nodal value of the magnetic vector potential, as shown in Figure 5. The magnetic vector potential waveform was formed by selecting the nodal value at a specific node number in the stator tooth and varying by one slot with the node index number over one period. The signal reformation up to  $5^{th}$  harmonic components provide relatively good accuracy. However, a significant distortion of the reformed signal is noticeable when the signal is composed of  $7^{th}$  harmonic component due to non-uniform step size. Thus, the lower harmonic components, i.e., up to  $5^{th}$  harmonic components, were chosen in the iron losses computation as shown in Figure 4.

In the case of dynamic analysis, the most significant harmonic components, i.e., up to  $9^{th}$  are depicted in Figure 4, and all the harmonic components were taken into account for the iron losses calculation. No even harmonic components ap-

pear in both the static and dynamic analysis as they cancel out each other because of the symmetrical flux density waveform. It can be seen that the flux density per harmonic components has an almost similar magnitude for both methods in Figure 4.

### C. Hysteresis and Eddy Current Loss Components

Hysteresis and eddy current loss per harmonic components in both methods are illustrated in Figure 6. Hysteresis loss is dominating in the fundamental frequency component. On the other hand, eddy current loss becomes more ruling at higher-order frequency components as the eddy current loss is proportional to the square of the harmonic frequency components. We understand that the flux density decomposition is more justifiable for the higher frequency components. However, the proposed method is limited to include the harmonic components of more than 250 Hz, the reason is already specified in Section III-B. The higher harmonic components were checked for the dynamic analysis up to 3000 Hz, and no significant hysteresis or eddy current loss components were found more than 450 Hz for the studied machine. Thus, no harmonic components were reported above 450 Hz.

The total stator iron loss as a contribution of hysteresis and eddy current loss is shown in Figure 6. The contribution of hysteresis loss is more in total stator core loss as eddy current loss is reduced due to the lamination and small thickness of the stator core sheets. The proposed method has a relatively good agreement with the time-stepping method. The loss difference between these two methods is found at 8.94%. The proposed method is slightly overestimating the iron losses, especially the losses in the fifth harmonic component compared to the losses compute from the dynamic analysis. The reason behind the overestimation is probably due to the fact that the accuracy of the Fourier coefficients calculation might drop because of the unevenly spaced samples. Moreover, less number of points were taken into account over one period might degrade the overall Fourier analysis performance as it provides a more accurate result when the number of samples is increased.

### D. Computational Cost

The iron losses computation from a single static field solution is much faster than the time-stepping simulation. The iron losses computation from a single static simulation costs 0.512 s; on the other hand, the time-stepping simulation requires 35.07 s for the same number of elements and nodes using an Intel-Xeon 3.4-GHz 16-GB-RAM workstation. The computation time for both methods is listed in Table I.

### E. Effect of Damper Windings, Supply Voltage Phase Shift and Rotor Angle Variation on Iron Losses

The effect of damper windings on the flux density harmonic reduction; consequently, the iron losses computation was studied for the dynamic analysis. The conductivity of the damper windings was set close to zero, in the case of dynamic

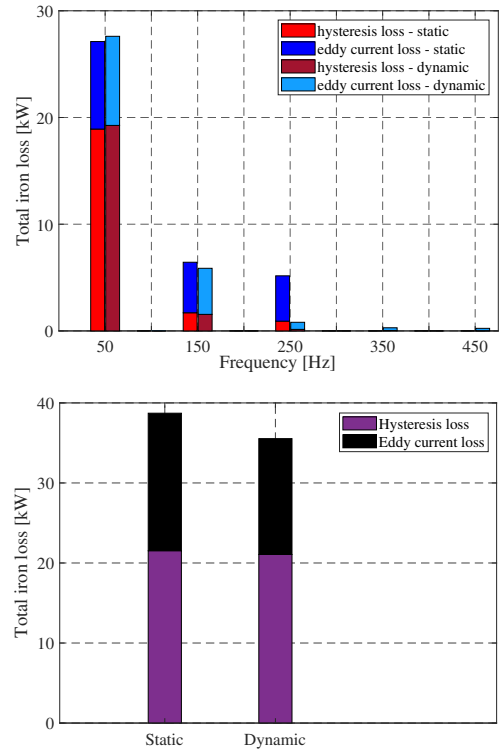


Fig. 6. Total iron loss comparison between the static and dynamic analysis: (above) hysteresis and eddy current loss per harmonic components; (below) contribution of hysteresis and eddy current losses in the total iron loss.

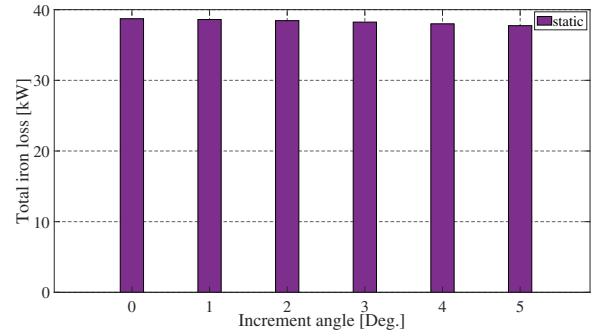


Fig. 7. Effects of the supply voltage phase shift and the relative angle of the rotor with respect to the stator slotting on the iron losses computation over one tooth pitch in the static analysis.

analysis, so that no current can induce in the bars. It was found that the inactivity of the damper windings significantly increases the rotor iron losses, particularly rotor eddy current loss, but there is no such effect noticed in the iron losses of the stator core for the dynamic analysis.

The effect of the supply voltage phase shift  $\phi$ , and the rotor angle  $\theta$  variation over one tooth pitch on the iron losses computation from a static field solution was also investigated. At first, the stator iron losses computed at a specific condition where the initial phase angle of the supply voltage and the rotor angle was  $\phi = 0$  and  $\theta = 31.9^\circ$ , respectively. Later, the phase angle  $\phi$  was varied from  $0^\circ$  to  $5^\circ$ , and the rotor

angle  $\theta$  was varied from  $31.9^\circ$  to  $36.9^\circ$  at the one-degree interval. It was found that the relative rotor position with respect to the stator slotting does not affect the terminal voltage, current, and power factor; however, the air gap torque and the output power is changed slightly. The stator iron losses are decreased slightly at each interval with increasing the supply voltage phase shift  $\phi$  and the rotor angle  $\theta$  as illustrated in Figure 7, which is maximum 2.5% compared to the computed iron losses at the initial position, i.e.,  $\phi = 0$  and  $\theta = 31.9^\circ$ ; hence, no significant effect was found. We are aware of the importance of computing the iron losses at multiple load points. The insignificant dependency of the proposed method with the variation of the rotor angle with respect to the stator slotting position increases our belief that the accuracy of the proposed method will remain stable for other loading conditions as well.

#### IV. CONCLUSION

A method of the iron losses computation in a synchronous machine from a static field solution has been proposed in this paper. The proposed method has relatively good accuracy compared to the dynamic analysis based method (8.94% maximum difference) and showed a high potentiality of the iron losses computation with a less computation cost over the conventional time-stepping method. The developed method can be highly productive and profitable for the iron losses calculation when an excessive number of computations are required, such as for machine optimization. Moreover, increasing the computational accuracy of the proposed method can substitute the time consuming conventional loss computation method in many applications. The accuracy of the developed loss computation technique can be improved by reconstructing the stator mesh, so that, every slot pitch meshes can be taken into account and forming a more densely mesh in order to attain more sampling points, which eventually increase the resolution of the flux density waveform. The utmost goal is to improve the accuracy of the Fourier decomposition of the flux density waveform, hence, the iron losses computation, which is our next step.

#### V. REFERENCES

- [1] S. J. Salon, *Finite Element Analysis of Electrical Machines*. Springer Science & Business Media, 2012.
- [2] A. Arkkio, "Analysis of induction motors based on the numerical solution of the magnetic field and circuit equations," PhD thesis, Helsinki University of Technology, Finland, 1987.
- [3] P. Hudák, V. Hrabovcová, P. Rafajdus, and J. Mihok, "Core loss analysis of the reluctance synchronous motor with barrier rotors," *Journal of Electrical Engineering*, vol. 55, no. 9-10, pp. 273–276, 2004.
- [4] K. Yamazaki and Y. Seto, "Iron loss analysis of interior permanent-magnet synchronous motors-variation of main loss factors due to driving condition," *IEEE Transactions on Industry Applications*, vol. 42, no. 4, pp. 1045–1052, 2006.
- [5] A. Belahcen, V. Mukherjee, M. F. Far, P. Rasilo, and M. Hinkkanen, "Coupled field and space-vector equations of bearingless synchronous reluctance machine," in *2016 XXII International Conference on Electrical Machines (ICEM)*. IEEE, 2016, pp. 2581–2587.
- [6] E. Dlala, "Comparison of models for estimating magnetic core losses in electrical machines using the finite-element method," *IEEE Transactions on Magnetics*, vol. 45, no. 2, pp. 716–725, 2009.

- [7] F. A. Fouad, T. Nehl, and N. Demerdash, "Magnetic field modeling of permanent magnet type electronically operated synchronous machines using finite elements," *IEEE Transactions on Power Apparatus and Systems*, no. 9, pp. 4125–4135, 1981.
- [8] R. Schifer and T. Lipo, "Core loss in buried magnet permanent magnet synchronous motors," *IEEE Transactions on Energy Conversion*, vol. 4, no. 2, pp. 279–284, 1989.
- [9] M. Al-Din, A. Kader, and J. Al-Samarai, "A new method to compute eddy current losses by the finite elements method," in *IAS'97. Conference Record of the 1997 IEEE Industry Applications Conference Thirty-Second IAS Annual Meeting*, vol. 1. IEEE, 1997, pp. 3–9.
- [10] D. M. Ionel and M. Popescu, "Finite-element surrogate model for electric machines with revolving field—application to ipm motors," *IEEE Transactions on Industry Applications*, vol. 46, no. 6, pp. 2424–2433, 2010.
- [11] G. Y. Sizov, D. M. Ionel, and N. A. Demerdash, "Modeling and parametric design of permanent-magnet ac machines using computationally efficient finite-element analysis," *IEEE Transactions on Industrial Electronics*, vol. 59, no. 6, pp. 2403–2413, 2011.
- [12] D. Kampen, M. Owzareck, S. Beyer, N. Parspour, and S. Schmitt, "Analytical core loss models for electrical steel in power electronic applications," in *2012 13th International Conference on Optimization of Electrical and Electronic Equipment (OPTIM)*. IEEE, 2012, pp. 109–117.
- [13] A. Arkkio and A. Niemenmaa, "Estimation of losses in cage induction motors using finite element techniques," in *IEEE International Conference of Electrical Machines*, 1992, pp. 317–321.
- [14] K. Ali, K. Atallah, and D. Howe, "Prediction of mechanical stress effects on the iron loss in electrical machines," *Journal of applied physics*, vol. 81, no. 8, pp. 4119–4121, 1997.
- [15] A. Belahcen and A. Arkkio, "Comprehensive dynamic loss model of electrical steel applied to fe simulation of electrical machines," *IEEE Transactions on Magnetics*, vol. 44, no. 6, pp. 886–889, 2008.
- [16] R. Kytomaki, A. Arkkio, A. Niemenmaa, and A. Suontausta, "Validity of conventional and modern methods of no-load loss calculation in asynchronous machines-statistic approach," in *1997 Eighth International Conference on Electrical Machines and Drives (Conf. Publ. No. 444)*. IET, 1997, pp. 185–189.
- [17] A. Boglietti, A. Cavagnino, M. Lazzari, and M. Pastorelli, "Predicting iron losses in soft magnetic materials with arbitrary voltage supply: An engineering approach," *IEEE Transactions on magnetics*, vol. 39, no. 2, pp. 981–989, 2003.

#### VI. BIOGRAPHIES

**Md Masum Billah** received the B.Sc. degree in electrical and electronic engineering from American International International University-Bangladesh (AIUB), Bangladesh, and the M.Sc. (Tech.) degree in automation and electrical engineering from Aalto University, Espoo, Finland in 2016 and 2020, respectively. Currently, he is working toward the D.Sc. degree in Aalto University, Department of Electrical Engineering and Automation.

**Floran Martin** received his D.Sc. degree from University of Nantes in 2013. He is currently working as a Post-doctoral researcher in Aalto University, Department of Electrical Engineering and Automation. His research is oriented toward magneto-mechanical effects in steel sheets and optimization of electrical machines.

**Anouar Belahcen** (M13-SM15) received the M.Sc. (Tech.) and Doctor (Tech.) degrees from Helsinki University of Technology, Finland, in 1998, and 2004, respectively. He is now Professor of electrical machines at Tallinn University of Technology, Estonia and Professor of Energy and Power at Aalto University, Finland. His research interest are numerical modelling of electrical machines, magnetic materials, coupled magneto-mechanical problems, magnetic forces, magnetostriction, and fault diagnostics.